Structural biology of *ex vivo* mammalian prions

Received for publication, May 10, 2022, and in revised form, June 16, 2022 Published, Papers in Press, June 23, 2022,
https://doi.org/10.1016/j.jbc.2022.102181

Efrosini Artikis[1], **Allison Kraus**[2,*], **and Byron Caughey**[1,*]

From the [1]*Laboratory of Persistent Viral Diseases, Rocky Mountain Laboratories, National Institute of Allergy and Infectious Diseases, National Institutes of Health, Hamilton, Montana, USA;* [2]*Department of Pathology, Case Western Reserve University School of Medicine, Cleveland, Ohio, USA*

Edited by Mike Shipston

The structures of prion protein (PrP)–based mammalian prions have long been elusive. However, cryo-EM has begun to reveal the near-atomic resolution structures of fully infectious *ex vivo* mammalian prion fibrils as well as relatively innocuous synthetic PrP amyloids. Comparisons of these various types of PrP fibrils are now providing initial clues to structural features that correlate with pathogenicity. As first indicated by electron paramagnetic resonance and solid-state NMR studies of synthetic amyloids, all sufficiently resolved PrP fibrils of any sort ($n > 10$) have parallel in-register intermolecular β-stack architectures. Cryo-EM has shown that infectious brain-derived prion fibrils of the rodent-adapted 263K and RML scrapie strains have much larger ordered cores than the synthetic fibrils. These bona fide prion strains share major structural motifs, but the conformational details and the overall shape of the fibril cross sections differ markedly. Such motif variations, as well as differences in sequence within the ordered polypeptide cores, likely contribute to strain-dependent templating. When present, N-linked glycans and glycophosphatidylinositol (GPI) anchors project outward from the fibril surface. For the mouse RML strain, these posttranslational modifications have little effect on the core structure. In the GPI-anchored prion structures, a linear array of GPI anchors along the twisting fibril axis appears likely to bind membranes *in vivo*, and as such, may account for pathognomonic membrane distortions seen in prion diseases. In this review, we focus on these infectious prion structures and their implications regarding prion replication mechanisms, strains, transmission barriers, and molecular pathogenesis.

Self-propagating prions cause fatal and transmissible spongiform encephalopathies in mammals. Classical transmissible spongiform encephalopathy or prion diseases involve the conversion of the host's normal cellular PrP (PrP^C) to aberrant infectious aggregates that have generically been called PrP^{Sc} (1). However, multiple abnormal PrP structures have been observed both *in vivo* and *in vitro*, and a key challenge is to determine which are relevant to disease, that is, infectious and/or toxic (2). Here, we will use the term PrP^d to refer to any disease-associated form of PrP regardless of its infectivity or pathogenicity (3). When histologically stained in infected brain tissue, PrP^d deposits can range from small, diffuse deposits to much larger extracellular amyloid plaques, with the relative amounts and distributions of such deposits being dependent on prion strain and host type (reviewed in (3)). For example, some prion diseases result in predominantly diffuse PrP^d deposits with little, if any, amyloid plaque while others have mixtures of both diffuse and plaque deposits. Still other types of prion disease have predominant amyloid plaques (4–6). Ultrastructural analyses using immunogold labeling have shown that PrP^d can accumulate not only as fibrils and amyloid plaques but also in forms that are not discernably fibrillar (reviewed in (3, 7)). Such forms are often closely associated with membranes that obscure visualization of PrP^d morphology. When PrP^d is extracted from tissues, it is typically found in the form of amyloid fibrils (8, 9); however, two-dimensional crystalline arrays and other nonfibrillar or subfibrillar ultrastructures have also been observed (10–16). Both fibrillar and subfibrillar structures have been linked to prion infectivity (14), but the structural relationships and pathophysiological roles of these various prion ultrastructures remain unclear.

The normal precursor to PrP^{Sc}, PrP^C, has substantial sequence homology among mammals (17) but its general physiological function(s) are uncertain. PrP^C has multiple ligands and plays roles in processes such as cellular differentiation, signaling, adhesion, stress tolerance, and redox activities (reviewed in (18–20)), suggesting a cell surface scaffolding function that organizes and mediates a variety of physiological functions (21). Unlike most proteins that are converted to pathologic oligomers and amyloids, PrP^C usually contains N-linked glycans (22, 23) and a glycophosphatidylinositol (GPI) anchor (24). In its native monomeric state, PrP^C has predominant intrinsically disordered and α-helical domains (reviewed in (25)). In contrast, PrP^{Sc} is multimeric (14, 26, 27), rich in β-sheet content (28–30), detergent-insoluble, and partially protease-resistant (31, 32) (a.k.a. PrP^{Res}). PrP^{Sc} multimers propagate by binding and refolding PrP^C as they elongate (26, 33). This type of propagation mechanism, whereby seeding overcomes a kinetic barrier between the native PrP^C state and the formation of ordered aggregates, is characteristic of PrP^{Sc}-based and other prion-like neurodegenerative diseases. A small subset (10%–15%) of human prion disease cases involve expression of PrP^C mutants with potentially altered folding and/or stability (34, 35), but most cases (*i.e.*, those with sporadic or acquired prion disease) express WT PrP^C.

* For correspondence: Byron Caughey, bcaughey@nih.gov; Allison Kraus, alk127@case.edu.

Although the steps are poorly understood, the exposure of PrP^{C} to the PrP^{Sc} template perturbs the canonical PrP^{C} folding pathway to allow complete refolding of the polypeptide chain (29, 30, 33, 36, 37). Detailed characterization of the structures involved is crucial in understanding the molecular pathogenesis of prion diseases and designing and/or screening for potentially therapeutic vaccines and conversion inhibitors.

We recently reported the first high-resolution structure of a fully infectious *ex vivo* prion (hamster 263K scrapie) (38, 39), and since then, structures of WT (40) and GPI-deficient (anchorless) (41) forms of another prion strain (mouse RML) have also been reported by Manka *et al.* and us. Here, we compare the available infectious prion structures to each other and to previously determined near-atomic structures for synthetic noninfectious fibrils. We also discuss implications for the molecular bases for prion pathogenesis, strain diversity, and transmission barriers.

Experimental underpinnings of initial parallel in-register and 4-rung β-solenoid models

Several experimental barriers have impeded attempts to solve the atomic structure of the bona fide prions. The tendency of tissue-derived prions to clump without forming regular three-dimensional crystalline arrays has prevented the determination of their detailed structures by X-ray or electron diffraction techniques. However, fiber diffraction data have provided clear evidence that infectious brain derived PrP^{Sc} fibrils have a regular ∼4.9 Å spacing of polypeptide strands perpendicular to the fibril axis (reviewed in (42)). This is a characteristic feature of amyloid fibrils formed by stacked β-strands. Methodological difficulties in the preparation of highly infectious synthetic prions using isotopically labeled recombinant PrP substrates hindered the solution of high-resolution structures by solid state NMR (ssNMR) spectroscopy. Nonetheless, ground-breaking electron paramagnetic resonance (EPR) and ssNMR studies of the protease-resistant cores of synthetic recombinant PrP fibrils first demonstrated that various recombinant PrP molecules can form fibrils in which the monomers are stacked parallel and in-register, that is, with residues of one monomer aligned immediately adjacent to the corresponding residues of the adjacent monomers (43–49). Based on these and other types of empirically derived lower-resolution data, parallel in-register intermolecular β-sheet/stack (PIRIBS) (Fig. 1) models of prion fibrils and strain permutations were proposed (45).

To accommodate the ∼135 to 150 residue protease-resistant core that is common in multiple PrP^{Sc} strains, such PIRIBS models require serpentine windings of the polypeptide chain to allow it to fit within the cross sectional dimensions of prion fibril cores (45). An alternative 4-rung β-solenoid (4RβS) model (Fig. 1) (42, 50, 51) for the GPI-anchorless RML (aRML) prion fibril was proposed based on observations of brain-derived prion fiber diffraction patterns, low-resolution cryo-EM, and other data. Key among those observations was evidence of repeating features along the fibril axis with a spacing of 19.2 Å in addition to the ∼4.9 Å spacing between strands within β-sheets (as is seen in the PIRIBS model). The 19.2 Å spacing along the axis of a protofilament was suggested to correspond to interfaces between monomers if each provided four successive rungs, as opposed to one in a PIRIBS architecture. The resulting 4RβS protofilament would be much narrower cross sectionally than the PIRIBS structure. Accordingly, whereas PIRIBS modeling posited that *ex vivo* prion fibrils were comprised of a single protofilament, the 4RβS fibril model suggested two intertwined protofilaments. Thus, the hypothesized PIRIBS and 4RβS fibril architectures were fundamentally different; however, prior to the last year and a half, no empirical data unequivocally discriminated between these architectures for bona fide infectious prions.

Recent advances in the field of cryo-EM have allowed for the atomic and near-atomic resolution of many macromolecular complexes (reviewed in (52, 53)). Conformational and compositional heterogeneity often precludes conventional methods of structure determination (such as NMR and X-ray crystallography) from resolving large biomolecular assemblies, membrane proteins, and systems with polymorphism (reviewed in (53)). When imaging with cryo-EM, careful sample preparation, preservation of important scaffolding molecules and cofactors, and proper vitrification may decrease haphazard clumping of amyloids and help produce grids with an adequate distribution of fibrillar assemblies (54). Advanced neural network algorithms can aid in particle picking, noise reduction, and image class averaging (55, 56). Helical reconstruction capabilities in analysis software such as RELION 3.1 (https://www3.mrc-lmb.cam.ac.uk/relion/index.php/Main_Page) (57–59) allow for the *de novo* modeling of fibrils from 3D reconstructions, and the acceleration of data processing with the usage of graphical processing units can further achieve higher resolution of structures (60).

Structures of synthetic PrP fibrils by cryo-EM

Significant insights into how PrP molecules can assemble into amyloid fibrils have come from cryo-EM studies of synthetic recombinant PrP fibrils. Such structures include fibrils of recombinant human PrP94 to 178 (rhu PrP94–178) (61) (Fig. 2*A*), full-length human PrP23 to 231 (rhu PrP23–231) (62) (Fig. 2*B*), mutant full-length human E196K PrP23 to 231 (rhu PrP23–231 E196 K) (63) (Fig. 2*C*), human PrP23 to 144 (rhu PrP23–144) (64), and a much shorter synthetic peptide (residues 168–176) of bank vole PrP (65). Importantly, the infectivity of these synthetic fibrils has not been documented to our knowledge. The protease-resistant cores are much smaller than those found in bona fide tissue-derived infectious PrP^{Sc} fibrils making it likely that these synthetic fibrils are either noninfectious or at least many orders of magnitude less infectious per unit protein (66–68). It is notable, however, that the murine homolog of the rhu PrP23–144 peptide has been shown to cause prion disease with a 100% attack rate in transgenic PrP-overexpressing mice (69). This murine PrP sample was not titered, but the long incubation periods were consistent with the titer being rather low relative to *ex vivo* prions.

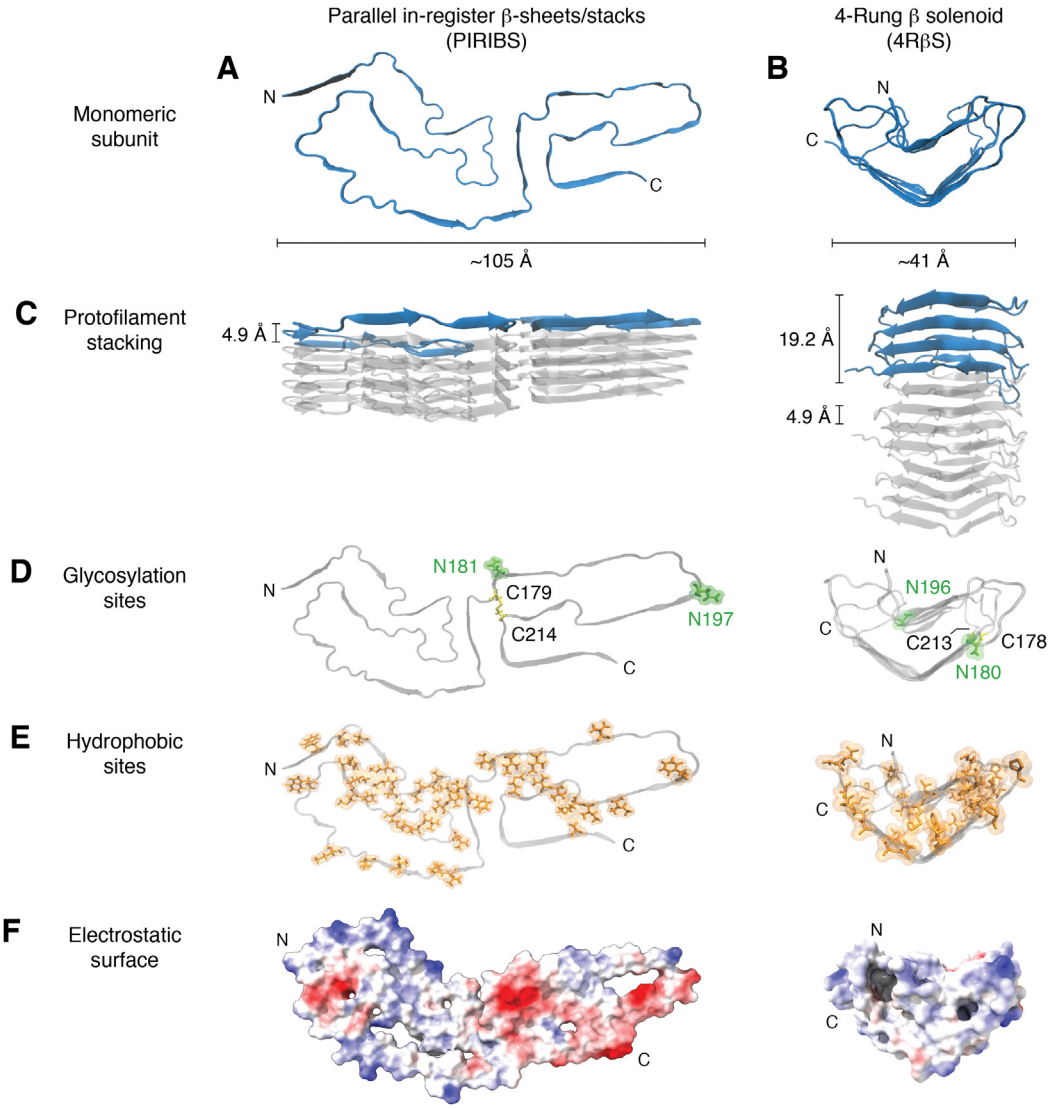

Figure 1. Recent models for prion fibrils. *A*, monomeric subunit of the 263K prion within its parallel in-register intermolecular β-sheet or stack (PIRIBS) architecture (38, 39). *B*, monomeric subunit within a 4-rung β-solenoid (4RβS) architecture hypothesized initially for the anchorless RML (aRML) prion (50), but see contrary data demonstrating PIRIBS architecture for this strain (41). Spacing of cross-β strands in both models is ∼4.9 Å (*C*). This is also the spacing of each monomer in the PIRIBS structure, whereas in the 4RβS model the monomers span 19.2 Å along the fibril axis (*C*). Glycosylation sites (*D*) at positions N181 and N197 (hamster numbering, PIRIBS) and N180 and N196 (mouse numbering, 4RβS) are labeled in *green* and a disulfide bond between C179 and C214 (PIRIBS) and C178 and C213 (4RβS) is colored in *yellow*. Note: an extra glycine residue at position 53 in the hamster PrP sequence shifts the hamster-mouse sequence alignment for subsequent residues. The lower panels show the distribution of hydrophobic residues in *orange* (*E*) and the electrostatic surface (*F*) (*red* and *blue* indicate negative and positive charges, respectively).

These various synthetic PrP fibrils all have PIRIBS architectures but with different sequences constituting their ordered fibrillar cores. In the rhu PrP94–178 fibrils, the core is formed by two closely packed, symmetrical protofilaments, with each protofilament core comprised of a β-arch of residues 106 to 145 (61). In this context, β-arch has been used to mean a hairpin-shaped motif in an amyloid cross section with a loop at its tip and intermolecular β-sheets on its flanks (61). Residues 106 to 145 also form the well-resolved core of fibrils of rhu PrP23–144 but assume a markedly distinct conformation and a four-protofilament assembly. This sequence corresponds to that expressed in humans with a form of Gerstmann–Sträussler–Scheinker syndrome linked to expression of PrP with the rare Y145Stop mutation (4, 70).

Rhu PrP23–231-derived fibrils also have two protofilaments but with ordered cores formed by C-terminal residues 170 to 229 (62). In contrast to the rhu PrP94–178 fibrils, the main feature of these protofilament cores is a β-arch linked at the base by the natural disulfide bond formed between Cys179 and Cys214. Importantly, this intramolecular disulfide bond is native to PrP^{C} and is known to be retained in the conversion to PrP^{Sc} (71–73). This disulfide β-arch is related to disulfide β-arches suggested previously by multiple EPR and ssNMR analyses of analogous synthetic human and rodent PrP fibrils (43, 44, 46, 48, 61, 62, 74). Rhu PrP23–231 E196K fibrils formed from PrP containing the familial human prion disease-linked E196K mutation have a PIRIBS architecture with an ordered core dominated by a disulfide β-arch (63). However, in this

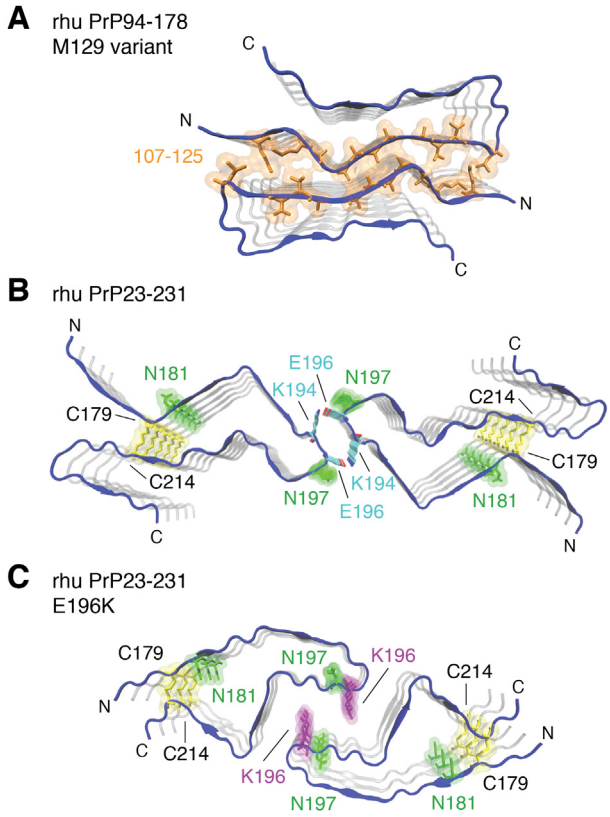

Figure 2. Ordered core structures of synthetic prion fibrils derived from cryo-EM. *A*, the two protofilaments of the rhu PrP94–178 (M129 variant) (61) are traced in *blue*. Hydrophobic residues at the interface of the two protofilaments are shown in *orange*. *B*, the two protofilaments of the rhu PrP23–231 fibril (62) with highlighted glycosylated sidechains (*green*) and disulfide bond (*yellow*). Salt-bridges formed between K194 and E196 at the interface of opposing protofibrils are colored by heteroatom (carbon, *cyan*; oxygen, *red*; nitrogen, *blue*). *C*, protofilaments of the E196K mutant (63) with highlighted as in glycosylated sidechains (*green*; N181 and N197), the disulfide bond (*yellow*; C179 and C214), and the E196K mutation (*purple*).

case the arch has a distinct conformation, providing evidence that the disulfide β-arch motif can vary between types of PrP fibrils.

Collectively, these studies of synthetic PrP fibrils demonstrated two major structural features. Firstly, recombinant C-terminally truncated PrP molecules tend to form PIRIBS-based amyloid fibrils with ordered cores spanning the central hydrophobic domain of residues ∼113 to 131 (46, 47, 49, 61, 75). Secondly, both full-length and N-terminally truncated PrP molecules can form fibrils with PIRIBS-based cores spanning residues ∼170 to 229, which are centered on disulfide-linked β-arches (43–45, 48, 62, 63). Fibrils of the latter type have been obtained *in vitro* with either spontaneous nucleation or initial seeding by tissue-derived PrP^{Sc} (45).

High-resolution cryo-EM analyses of infectious tissue-derived prion fibrils

Three high-resolution cryo-EM structures of fully infectious, brain-derived prion fibrils have now been reported (38–41). These include the hamster-adapted scrapie strain 263K (Fig. 3*A*) (38, 39) and both WT (40) and GPI-anchorless (Fig. 3*B*) (41) forms of the mouse RML scrapie strain. Animal bioassays demonstrated that each of these bona fide PrP^{Sc} (PrP^{Res}) preparations contained roughly a billion 50% lethal doses (LD_{50}) per milligram protein. The WT 263K and RML prions also have GPI anchors and abundant N-linked glycans. In contrast to the synthetic fibrils reviewed above, these *ex vivo* prions have much larger proteinase K–resistant cores spanning from residues ∼81–90 to ∼231. Indeed, this span of core residues is also larger than those of most, if not all, other neuropathologic PIRIBS-based protein amyloids, such as those composed of Aβ (76) and tau (77).

Like the synthetic PrP amyloids, each of these *ex vivo* prion fibril structures has PIRIBS cores. However, commensurate with the latter's much larger protease-resistant cores, the span of residues that form their highly resolved PIRIBS cores is more than twice that seen in the synthetic fibrils. Specifically, the 263K, wtRML, and aRML fibril cores span residues 95 to 227 (38), 94 to 225 (40), and 93 to 230 (41), respectively. With these much larger PIRIBS cores, single monomers span the entire fibril cross section (Fig. 3, *A* and *B*). Morphologic analyses of the wtRML (40) and aRML (41) preparations detected a small proportion of paired fibrils (*e.g.*, ∼10% of wtRML), but such duplexes were not regular enough to be resolved as a discrete subpopulation by single particle analysis of any of the brain-derived prion preparations. While the aRML and wtRML fibril cross sections are quite similar, they are both more acutely V-shaped than the 263K cross section (compare Fig. 3, *A* and *B*). It had long been assumed, based primarily on negatively stained transmission electron microscopy images, that prion fibrils or rods were comprised of two protofilaments. However, we now suspect that what appeared to be separation between two protofilaments was actually deposition of stain in the trough of the "V" between the N- and C-terminal lobes of the fibril structure as we suggested earlier (45).

The two types of β-arch motifs that are seen in synthetic fibrils, namely those spanning approximately residues 113 to 131 and 170 to 229, are also found in the 263K (38, 39) and RML prions (40, 41) (Fig. 3, *A*–*C*); however, whereas the synthetic fibrils have either one or the other of these N- or C-proximal β-arches, the much larger cores of *ex vivo* prions have both arches at once. We provisionally refer to the more N-terminal of these β-arches as the "N β-arch" (Fig. 3, *A*–*C*) and the C-terminal one as the "disulfide β-arch" (Fig. 3, *A* and *B*, *D*) with reference to the disulfide bond at its base. Another more central β-arch, which shares its N-terminal flank with the N β-arch, is called the middle β-arch (Fig. 3, *A* and *B*, *E*). Still another key feature of the 263K and RML prions is a steric zipper (Fig. 3*E*) that holds the extreme N-terminal residues of the core against the head of the middle β-arch. This steric zipper involves the tight interdigitation of the sidechains of alternating residues (*blue*), which are homologous in the hamster and mouse PrP sequences. Steric zippers have been observed in the spines of multiple amyloid fibrils (78–80).

Although the 263K and RML prion structures share structural motifs that, in the cases of the N β-arches and disulfide β-arches, overlap those seen previously in various synthetic PrP fibrils, their conformational details are substantially different

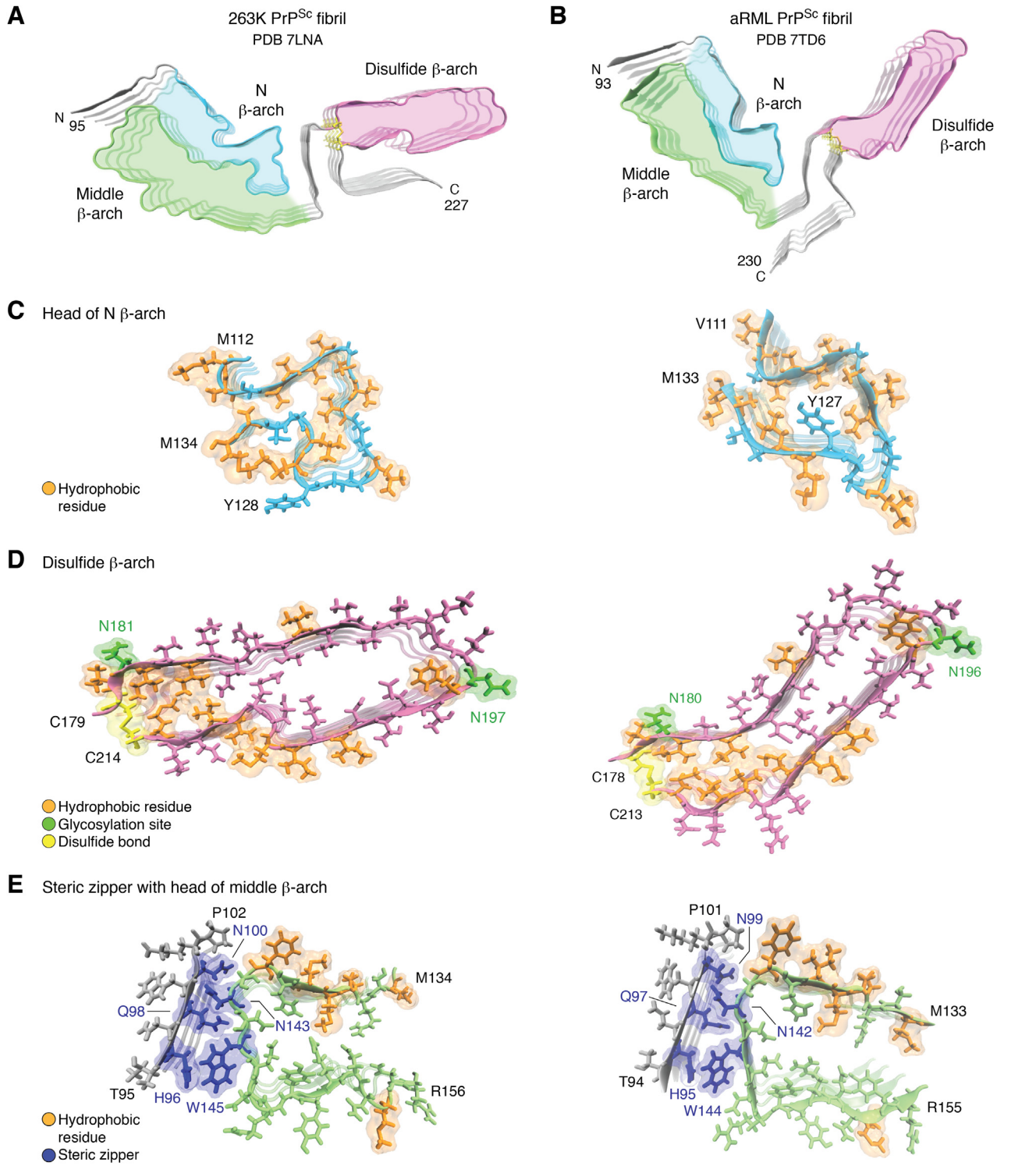

Figure 3. Comparison of 263K and aRML prion structures. Cross-sections of the (*A*) 263K and (*B*) aRML fibril (4-monomer segments) highlighting analogous β-arch motifs (N β-arch, *cyan*; middle β-arch, *green*; disulfide β-arch, *pink*). *C*, tips of N β-arches of 263K (left) and aRML (right) with hydrophobic residues in *orange*. *D*, disulfide β-arches (*pink*) with respective disulfide bonds (*yellow*), glycosylation sites (*green*), and hydrophobic residues (*orange*). *E*, steric zippers (*blue*) formed between tips middle β-arches and respective N-terminal residues. The 263 K structure illustrated in this figure includes residues 194 to 196 which were not specified in PDB ID 7LNA. aRML, anchorless RML; PDB, Protein Data Bank.

from the latter and each other (38–41). For example, the heads of the N β-arches of 263K (Fig. 3*A*) and RML (Fig. 3*B*) fibrils have strikingly different anvil- or mushroom-shaped heads despite having identical glycine and hydrophobic amino acid sequences spanning residues 113 to 138 (hamster numbering) (Fig. 3*C*). Perhaps sequence differences that are immediately N- and C-terminal to this head region differentially influence the folding of the intervening or proximal residues.

Strain-dependent conformational differences are also striking in the C-terminal half of the prion fibril cores (38–

41). Specifically, the disulfide β-arches (Fig. 3*D*) of the RML strains are almost perpendicular to the N β-arch, while in 263K these two β-arches are nearly aligned. The extreme C termini are also quite distinct. In 263K, the C-terminal linkage to the GPI anchor closely flanks the disulfide β-arch while in the RML structures, these residues project in the opposite direction (Fig. 3, *A* and *B*). Comparison of the aRML and wtRML structures also indicates that, whereas the ordered core of aRML spans residues 93 to 230, the wtRML core extends only to residue 225. The less-ordered extreme C terminus of wtRML likely relates to the presence of the structurally heterogeneous GPI anchors, which are absent on aRML.

Overall, comparison of the 263K and the RML strains reveals that their fibrillar cross sections, and hence, growth templates, are distinct. Given that the hamster and mouse PrP sequences differ at eight positions within the fibril core, some of the difference between the 263K and RML prion conformation may be influenced by sequence as aforementioned. Clearer demonstrations of the purely conformational determinants of prion strain will require high-resolution analyses of strains isolated from hosts of the same genotype.

Finally, we note that a PIRIBS fibril architecture has recently been posted for highly infectious synthetic prions formed *in vitro* from bank vole PrP (109I) 23 to 231 based on PITHIRDS solid-state NMR analyses (74). This work adds significantly to the small, but growing, list of PIRIBS-based fully infectious prion structures.

Conversion of PrP^C to PrP^{Sc}

Presumably, the conformational conversion and incorporation of incoming PrP monomers or, perhaps, preformed oligomeric intermediates occurs on the ends of the prion fibrils (38, 39). The sequence of events in the refolding of PrP^C and the extent to which that each of those events is guided directly by interactions with the PrP^{Sc} template are far from clear. However, comparison of the conformations of the hamster PrP^C (*e.g.* (81)) and PrP^{Sc} (38) structures indicates that an entire restructuring of PrP^C is required (Fig. 4), including elimination of all original tertiary structure, unfurling of the three α-helices, and dismantling of the small intermolecular β1-β2 sheet (38, 39). Formed in their place are extensive intermolecular β-sheets running parallel to the fibril axis with interspersed loops to form β-arches as well as other features of the tightly packed fibril core. Key among the required conversion steps would be the dissociation of PrP^C's β1-helix 1–β2 loop from the hairpin formed by helices 2 and 3 (Fig. 4, "Speculative intermediate"), a process that has been predicted and described as a "banana-peeling model" (82). As noted previously, the disulfide bond remains intact throughout the conversion process (71–73), consistent with conversion occurring in oxidizing environments such as the cell surface, endosomes, or extracellular spaces (6, 83–87).

Lateral views of the templating surfaces at each end of the 263K and RML fibrils show that polypeptide chains of the monomers are not entirely coplanar, with, for example, the hydrophobic heads of the respective N β-arch motifs protruding at one end and receding at the other (Fig. 4, upper right inset) (38–41). It is possible that at the protruding end, an interaction between this sticky head and the analogous residues of PrP^C, or a partially unfolded intermediate, might initiate refolding. Thereafter, sequential refolding and intermolecular backbone hydrogen bonding might follow along the "track" of the templating polypeptide backbone toward the N and C termini. We anticipate that PrP^C-to-PrP^{Sc} conversion process will also be influenced crucially by interactions with polyanionic cofactors (Fig. 4, middle inset), which have been shown to be important (88–95), and membranes, with the latter presumably being orchestrated primarily by GPI anchoring (96–99).

PrP^{Sc} glycans and GPI anchors—implications

Many previous studies have shown that PrP^{Res} glycoform patterns can vary systematically between prion strains within a given type of host and that such characteristic variations can be used to differentiate strains. For example, different subtypes of human sporadic Creutzfeldt–Jacob disease are discriminated in part based on glycoform patterns on immunoblots of brain-derived PrP^{Res} (reviewed in (100)). As noted above, the N-linked glycans and GPI anchors are displayed on the surfaces of 263K and wtRML fibrils, with potentially far-reaching implications in prion pathogenesis (38, 39). Studies of several different prion strains in WT mice *versus* transgenic mice expressing only GPI-anchorless PrP^C have also demonstrated profound roles of the GPI group on disease phenotypes (5, 6, 101–103). Without GPI anchors, as in prion-infected anchorless PrP transgenic mice or humans expressing anchorless PrP mutants, such as Y145X 163X, Y226X, Q227X, and G131V (104), PrP^{Sc} is free to accumulate in the large extracellular amyloid plaques that are prominent in such hosts. However, these posttranslational modifications do not seem to substantially alter the core structures of at least three murine prions strains, as probed by infrared spectroscopy (105). Also, the RML strain has been shown to maintain its fundamental strain characteristics such as incubation period and neuropathological lesion profile when passaged from WT mice to anchorless PrP mice and back again. However, two studies have described more subtle effects of passage of RML prions through anchorless mice with respect to their sensitivity to inhibitors in a cell panel assay (106) and the exposure of histidines 176 and 186 to H/D exchange with solvent (107). Nonetheless, the fact that the aRML and wtRML cryo-EM–based structures are similar to one another, yet different from the 263K structure, is consistent with prion core structures enciphering the primary properties of strains. However, clearly, the phenotypes of those strains can be further modulated markedly by the availability, or lack thereof, of GPI anchors and glycans in a given type of host or tissue

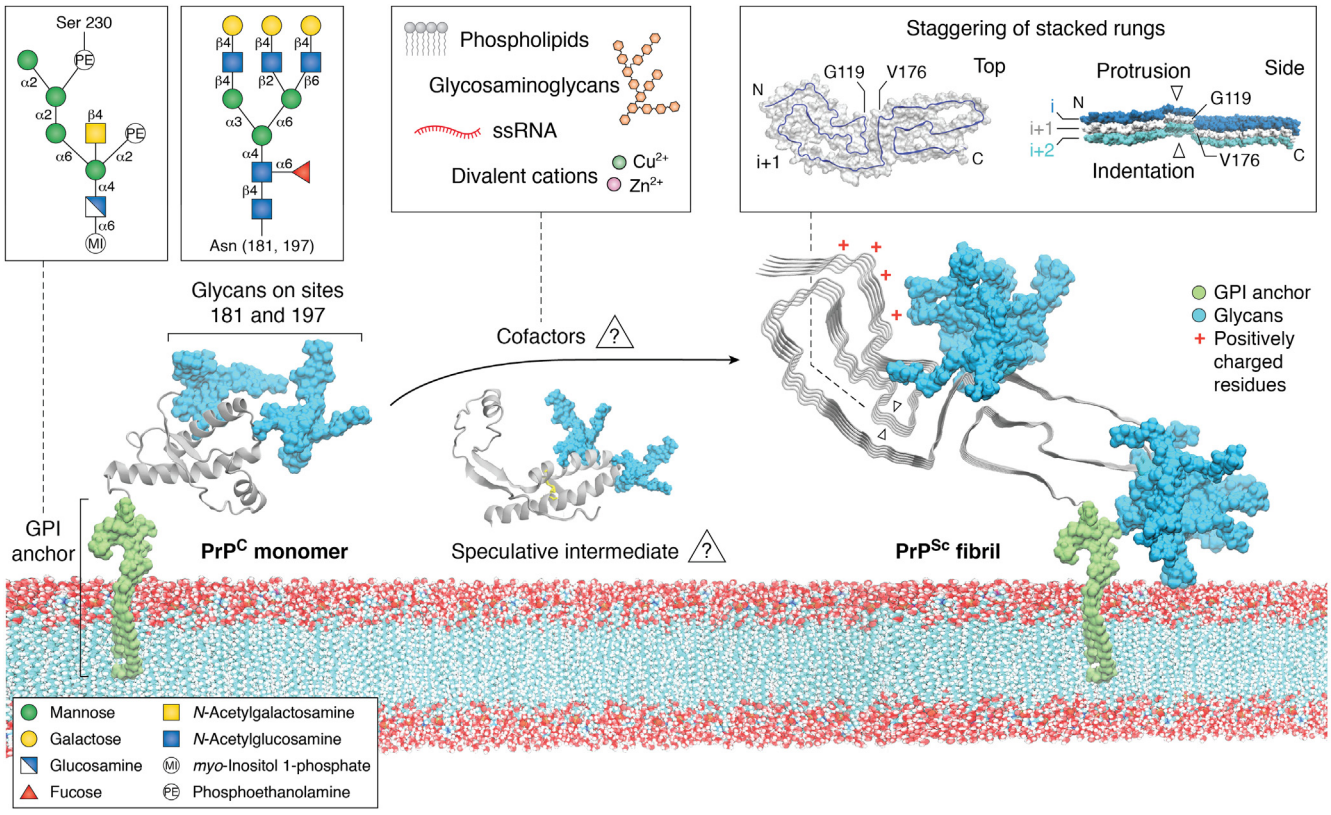

Figure 4. Conversion of PrP^{C} to PrP^{Sc}. Schematic of membrane bound PrP^{C} (only the ordered C-terminal domain determined by solution NMR (81) is shown) with GPI-anchor (*green*) and N-linked glycan moieties (*blue*) in POPC lipid bilayer. Insets depict representative GPI anchors and glycans. Membrane-bound 263K pentamer is shown with N-linked glycans (*blue*) and GPI anchor (*green*) determined by cryo-EM (39). A cluster of positively charged residues near the N terminus is marked with *red asterisks*. The inset on the right shows top view of a single polypeptide chain with arrows at positions G119 and V179 (left) and a side view of three stacked monomers (*silver*, *blue*, and *purple*) exhibiting fibril staggering and the diagonal orientation of G119 and V179 of the *silver* monomer. Also shown is a speculative conversion intermediate with PrP^{C}'s β1–helix 1-β2 loop peeled away from helices 2 & 3 (113) as well as an inset listing types of cofactors that can affect prion propagation *in vitro* (88, 89, 91–93) and might therefore be peripherally associated with prion fibrils. GPI, glycophosphatidylinositol.

(5, 6, 101, 104, 108–112). Importantly, both anchorless and GPI-anchored PrP^{Sc} can be infectious and capable of killing the host with equal speed (107).

The outward display of glycans and GPI anchors on the 263K (Fig. 4) and wtRML fibrils suggests that they could strongly modulate the interactions of prions with their environments *in vivo*. In particular, blanketing of at least the C-terminal half of the fibril cores with glycans and tethered membranes should severely restrict the access of other macromolecules (38). Macromolecules of particular significance might include proteostatic or innate immune factors involved in prion recognition and clearance. We also have proposed that pathognomonic PrP^{d}-associated membrane distortions that are observed in prion diseases might be due to attachment of membranes to PrP^{Sc} fibrils *via* the array of GPI anchors as they follow the twist of the fibril. Such distortions include invaginations, protrusions, and spiral membrane inclusions, any of which might disrupt cellular functions. The spreading of prions *via* membranous particles such as exosomes and tunneling nanotubes (7, 113–115) might also be facilitated by GPI-meditated tethering. A direct comparison of spreading mechanisms in WT and anchorless PrP mouse models after microinjections of 22L prions into the brain demonstrated profound differences. In WT mice spreading primarily followed neuronal circuitry, whereas in anchorless PrP mice, spread was slower and involved the brain interstitial fluid drainage system (102, 116). Moreover, neuroinvasion and neural spread of prion infection from the periphery are highly dependent on the presence of GPI-anchored PrP (101).

Species/transmission barriers mechanisms

An important issue in coping with prion diseases is the extent to which prion disease strain in one host species might infect other hosts with different PrP amino acid sequences. A most troubling example of interspecies transmission was the bovine spongiform encephalopathy epidemic in cattle that gave rise to variant Creutzfeldt–Jacob disease in humans (reviewed in (117)). There are analogous concerns about the possibility of chronic wasting disease causing prion disease in humans who hunt, eat, and/or are otherwise exposed to infected cervids (117–119). Also of concern are transmissions between nonhuman animal species, particularly, those of significance in agriculture and wildlife management. Many studies have shown that differences in PrP sequence between the infecting prion and the host's PrP^{C} can range from being inconsequential to being responsible for profound

transmission barriers (120–126). Even a single mismatch may make a host highly resistant to infection with certain prion strains (127–130). The availability of the 263K cryo-EM structure has allowed us to suggest a plausible mechanism for one such species barrier, that is, between hamsters and mice (38). When considered together, prior studies in transgenic mice (126) and cell cultures (131) have indicated that most important sequence mismatch in this transmission barrier was at residue 155 (hamster numbering), which is N in hamsters and Y in mice (Fig. 5). *In silico* modeling based on the 263K structure indicated that insertion of the bulkier Y sidechain into the space occupied by the N in the 263K structure would lead to steric clashes and require longer–range adjustments in polypeptide backbone of a hybrid prion structure (38). Although the PrP^{C} conversion mechanism at the PrP^{Sc} templating surface has not been defined, clashes at residue 155 appear likely to affect the kinetics of conversion and/or the stability of the product in a way that strongly restricts the ability of hamster 263K prions to grow and propagate when inoculated into mice. However, other less direct factors that have not yet been explored might also play roles in this species barrier mechanism.

Interestingly, many of the other sequence mismatches between the hamster and mouse PrP sequences are much less inhibitory (126, 131). Tolerance of these mismatches can be rationalized as being the consequence of those residues being outside the fibril core, on the surface, or in positions within the core where their sidechains would not subject to steric clashes or other destabilizing forces. More generally, considering the known diversity in the PrP sequence mismatches that influence the relative interspecies transmissibilities of prions and the conformational diversity between prion strains, it seems likely that the mechanisms involved will be manifold.

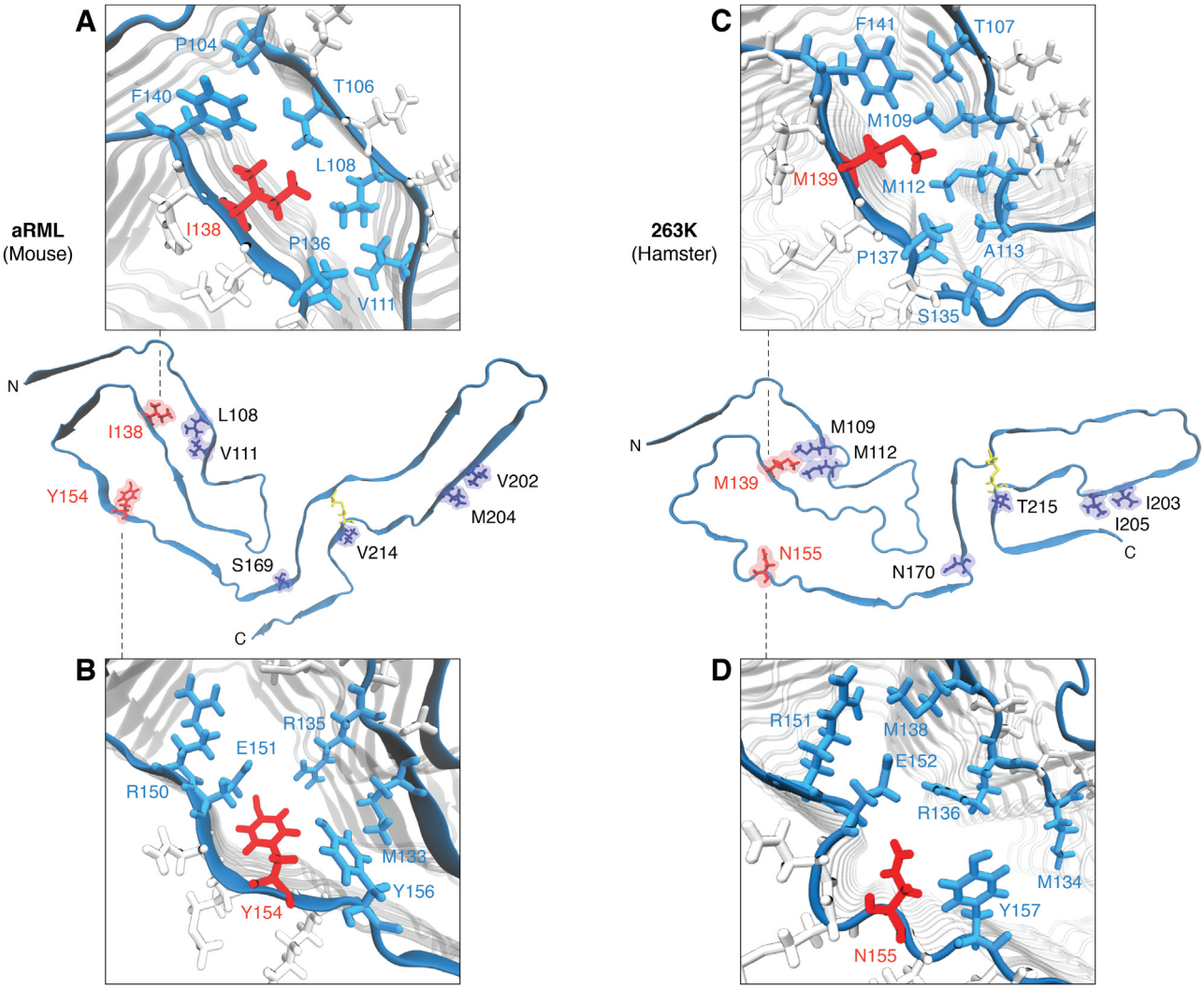

Figure 5. Potential transmission barrier mechanisms. Sidechain representations (*purple*, *red*) of the eight residue variations between mouse and hamster sequences are displayed on the monomer chains (aRML and 263K, respectively). Two residues (mouse: I138, Y154; hamster: M139, N155) implicated in cross species barrier mechanisms are displayed in *red*. Insets show mouse residues I138 (*A*) and Y154 (*B*) and corresponding hamster resides M139 (*C*) and N155 (*D*) and their sidechain orientations relative to those of neighboring residues (*cyan*) and give insight into the surrounding chemical environment. aRML, anchorless RML.

Conclusions

At this early stage, all of the available near-atomic structures of both highly infectious prions and much less pathogenic synthetic PrP fibrils are fibrillar with PIRIBS architectures. Many types of PrP-based prions exist in mammals, and further studies will be needed to determine the full range of prion structures. The increasing availability of such structures allows for more insight into the outstanding questions of the prion field. Already, we can see a tendency of PrP molecules in PIRIBS fibrils to form β-arch structural motifs that involve analogous sequences but vary in their detailed conformations. Variations in the conformations and relative positioning of these common β-arch motifs and other structural features can create specific conformational templates for the refolding and incorporation of PrP^C molecules, providing a molecular basis for the faithful propagation of distinct mammalian prion strains. The tight packing observed in certain regions of the 263K prion cores, together with molecular modeling, suggest a molecular basis for the 263K prion transmission barrier between hamsters and mice. Finally, the availability of near-atomic authentic prion structures should aid in the rational design and screening of drugs or vaccines that can interfere with pathological conversions of PrP^C to PrP^d, as well as strategies to promote detoxification and/or clearance of prions in infected individuals.

Acknowlegments—This work was supported in part by the Intramural Research Program of the NIAID, Mary Hilderman Smith, Zoë Smith Jaye, and Jenny Smith Unruh in memory of Jeffrey Smith; and the Britton Fund, and CWRU School of Medicine.

Author contributions—B. C., E. A., and A. K. conceptualization; B. C. writing–original draft; B. C., E. A., and A. K. writing–review & editing; E. A. visualization.

Conflict of interest—The authors declare that they have no conflicts of interest with the contents of this article.

Abbreviations—The abbreviations used are: 4RβS, 4-rung β-solenoid; aRML, anchorless RML; GPI, glycophosphatidylinositol; PIRIBS, parallel in-register intermolecular β-sheet/stack; ssNMR, solid state NMR.

References

1. Prusiner, S. B. (1998) Prions. *Proc. Natl. Acad. Sci. U. S. A.* **95**, 13363–13383
2. Caughey, B., and Kraus, A. (2019) Transmissibility *versus* pathogenicity of Self-propagating protein aggregates. *Viruses* **11**, 1044
3. Jeffrey, M., McGovern, G., Siso, S., and Gonzalez, L. (2011) Cellular and sub-cellular pathology of animal prion diseases: Relationship between morphological changes, accumulation of abnormal prion protein and clinical disease. *Acta Neuropathol.* **121**, 113–134
4. Ghetti, B., Piccardo, P., Spillantini, M. G., Ichimiya, Y., Porro, M., Perini, F., *et al.* (1996) Vascular variant of prion protein cerebral amyloidosis with tau-positive neurofibrillary tangles: The phenotype of the stop codon 145 mutation in PRNP. *Proc. Natl. Acad. Sci. U. S. A.* **93**, 744–748
5. Chesebro, B., Race, B., Meade-White, K., LaCasse, R., Race, R., Klingeborn, M., *et al.* (2010) Fatal transmissible amyloid encephalopathy: a new type of prion disease associated with lack of prion protein membrane anchoring. *PLoS Pathog.* **6**, e1000800
6. Chesebro, B., Trifilo, M., Race, R., Meade-White, K., Teng, C., LaCasse, R., *et al.* (2005) Anchorless prion protein results in infectious amyloid disease without clinical scrapie. *Science* **308**, 1435–1439
7. Caughey, B., Baron, G. S., Chesebro, B., and Jeffrey, M. (2009) Getting a grip on prions: oligomers, amyloids, anchors and pathological membrane interactions. *Annu. Rev. Biochem.* **78**, 177–204
8. Merz, P. A., Somerville, R. A., Wisniewski, H. M., and Iqbal, K. (1981) Abnormal fibrils from scrapie-infected brain. *Acta Neuropathol.* **54**, 63–74
9. Diringer, H., Gelderblom, H., Hilmert, H., Özel, M., Edelbluth, C., and Kimberlin, R. (1983) Scrapie infectivity, fibrils and low molecular weight protein. *Nature* **306**, 476–478
10. Wille, H., Govaerts, C., Borovinskiy, A., Latawiec, D., Downing, K. H., Cohen, F. E., *et al.* (2007) Electron crystallography of the scrapie prion protein complexed with heavy metals. *Arch. Biochem. Biophys.* **467**, 239–248
11. Govaerts, C., Wille, H., Prusiner, S. B., and Cohen, F. E. (2004) Evidence for assembly of prions with left-handed beta-helices into trimers. *Proc. Natl. Acad. Sci. U. S. A* **101**, 8342–8347
12. Wille, H., Michelitsch, M. D., Guenebaut, V., Supattapone, S., Serban, A., Cohen, F. E., *et al.* (2002) Structural studies of the scrapie prion protein by electron crystallography. *Proc. Natl. Acad. Sci. U.S.A* **99**, 3563–3568
13. Wille, H., and Prusiner, S. B. (1999) Ultrastructural studies on scrapie prion protein crystals obtained from reverse micellar solutions. *Biophys. J.* **76**, 1048–1062
14. Silveira, J. R., Raymond, G. J., Hughson, A. G., Race, R. E., Sim, V. L., Hayes, S. F., *et al.* (2005) The most infectious prion protein particles. *Nature* **437**, 257–261
15. Vanni, I., Pirisinu, L., Acevedo-Morantes, C., Kamali-Jamil, R., Rathod, V., Di Bari, M. A., *et al.* (2020) Isolation of infectious, non-fibrillar and oligomeric prions from a genetic prion disease. *Brain* **143**, 1512–1524
16. Cortez, L. M., Nemani, S. K., Duque Velásquez, C., Sriraman, A., Wang, Y., Wille, H., *et al.* (2021) Asymmetric-flow field-flow fractionation of prions reveals a strain-specific continuum of quaternary structures with protease resistance developing at a hydrodynamic radius of 15 nm. *PLoS Pathog.* **17**, e1009703
17. Watts, J. C., and Westaway, D. (2007) The prion protein family: diversity, rivalry, and dysfunction. *Biochim. Biophys. Acta* **1772**, 654–672
18. Caughey, B., and Baron, G. S. (2006) Prions and their partners in crime. *Nature* **443**, 803–810
19. Sigurdson, C. J., Bartz, J. C., and Glatzel, M. (2019) Cellular and molecular mechanisms of prion disease. *Annu. Rev. Pathol. Mech. Dis.* **14**, 497–516
20. Biasini, E., Turnbaugh, J. A., Unterberger, U., and Harris, D. A. (2012) Prion protein at the crossroads of physiology and disease. *Trends Neurosci.* **35**, 92–103
21. Linden, R. (2017) The biological function of the prion protein: a cell surface scaffold of signaling modules. *Front. Mol. Neurosci.* **10**, 77
22. Bolton, D. C., Meyer, R. K., and Prusiner, S. B. (1985) Scrapie PrP 27-30 is a sialoglycoprotein. *J. Virol.* **53**, 596–606
23. Multhaup, G., Diringer, H., Hilmert, H., Prinz, H., Heukeshoven, J., and Beyreuther, K. (1985) The protein component of scrapie-associated fibrils is a glycosylated low molecular weight protein. *EMBO J.* **4**, 1495–1501
24. Stahl, N., Borchelt, D. R., Hsiao, K., and Prusiner, S. B. (1987) Scrapie prion protein contains a phosphatidylinositol glycolipid. *Cell* **51**, 229–240
25. Wüthrich, K., and Riek, R. (2001) Three-dimensional structures of prion proteins. *Adv. Protein Chem.* **57**, 55–82
26. Caughey, B., Kocisko, D. A., Raymond, G. J., and Lansbury, P. T., Jr. (1995) Aggregates of scrapie-associated prion protein induce the cell-free conversion of protease-sensitive prion protein to the protease-resistant state. *Chem. Biol.* **2**, 807–817

27. Caughey, B., Raymond, G. J., Kocisko, D. A., and Lansbury, P. T., Jr. (1997) Scrapie infectivity correlates with converting activity, protease resistance, and aggregation of scrapie-associated prion protein in guanidine denaturation studies. *J. Virol.* **71**, 4107–4110
28. Caughey, B. W., Dong, A., Bhat, K. S., Ernst, D., Hayes, S. F., and Caughey, W. S. (1991) Secondary structure analysis of the scrapie-associated protein PrP 27-30 in water by infrared spectroscopy. *Biochemistry* **30**, 7672–7680
29. Safar, J., Roller, P., Gajdusek, D., and Gibbs, C., Jr. (1993) Conformational transitions, dissociation, and unfolding of scrapie amyloid (prion) protein. *J. Biol. Chem.* **268**, 20276–20284
30. Pan, K.-M., Baldwin, M., Nguyen, J., Gasset, M., Serban, A., Groth, D., *et al.* (1993) Conversion of alpha-helices into beta-sheets features in the formation of the scrapie prion proteins. *Proc. Natl. Acad. Sci. U. S. A.* **90**, 10962–10966
31. McKinley, M. P., Bolton, D. C., and Prusiner, S. B. (1983) A protease-resistant protein is a structural component of the scrapie prion. *Cell* **35**, 57–62
32. Caughey, B., Neary, K., Buller, R., Ernst, D., Perry, L., Chesebro, B., *et al.* (1990) Normal and scrapie-associated forms of prion protein differ in their sensitivities to phospholipase and proteases in intact neuroblastoma cells. *J. Virol.* **64**, 1093–1101
33. Kocisko, D. A., Come, J. H., Priola, S. A., Chesebro, B., Raymond, G. J., Lansbury, P. T., *et al.* (1994) Cell-free formation of protease-resistant prion protein. *Nature* **370**, 471–474
34. Vanik, D. L., and Surewicz, W. K. (2002) Disease-associated F198S mutation increases the propensity of the recombinant prion protein for conformational conversion to scrapie-like form. *J. Biol. Chem.* **277**, 49065–49070
35. Apetri, A. C., Vanik, D. L., and Surewicz, W. K. (2005) Polymorphism at residue 129 modulates the conformational conversion of the D178N variant of human prion protein 90– 231. *Biochemistry* **44**, 15880–15888
36. Bessen, R. A., Kocisko, D. A., Raymond, G. J., Nandan, S., Lansbury, P. T., Jr., and Caughey, B. (1995) Nongenetic propagation of strain-specific phenotypes of scrapie prion protein. *Nature* **375**, 698–700
37. Horiuchi, M., Chabry, J., and Caughey, B. (1999) Specific binding of normal prion protein to the scrapie form via a localized domain initiates its conversion to the protease-resistant state. *EMBO J.* **18**, 3193–3203
38. Kraus, A., Hoyt, F., Schwartz, C. L., Hansen, B., Artikis, E., Hughson, A. G., *et al.* (2021) High-resolution structure and strain comparison of infectious mammalian prions. *Mol. Cell* **81**, 4540–4551.e6
39. preprint Kraus, A., Hoyt, F., Schwartz, C. L., Hansen, B., Hughson, A. G., Artikis, E., *et al.* (2021) Structure of an infectious mammalian prion. *bioRxiv*. https://doi.org/10.1016/j.molcel.2021.08.011
40. Manka, S. W., Zhang, W., Wenborn, A., Betts, J., Joiner, S., and Saibil, H. R. (2022) 2.7 Å cryo-EM structure of *ex vivo* RML prion fibrils. *Nat. Commun.* In press
41. Hoyt, F., Standke, H. G., Artikis, E., Schwartz, C. L., Hansen, B., Li, K., *et al.* (2022) Structure of anchorless RML prion reveals motif variation between strains. *Nat. Commun.* In press
42. Wille, H., and Requena, J. R. (2018) The structure of PrP(Sc) prions. *Pathogens* **7**, 20
43. Cobb, N. J., Sonnichsen, F. D., McHaourab, H., and Surewicz, W. K. (2007) Molecular architecture of human prion protein amyloid: a parallel, in-register beta-structure. *Proc. Natl. Acad. Sci. U. S. A* **104**, 18946–18951
44. Cobb, N. J., Apetri, A. C., and Surewicz, W. K. (2008) Prion protein amyloid formation under native-like conditions involves refolding of the C-terminal alpha-helical domain. *J. Biol. Chem.* **283**, 34704–34711
45. Groveman, B. R., Dolan, M. A., Taubner, L. M., Kraus, A., Wickner, R. B., and Caughey, B. (2014) Parallel in-register intermolecular beta-sheet architectures for prion-seeded prion protein (PrP) amyloids. *J. Biol. Chem.* **289**, 24129–24142
46. Theint, T., Nadaud, P. S., Aucoin, D., Helmus, J. J., Pondaven, S. P., Surewicz, K., *et al.* (2017) Species-dependent structural polymorphism of Y145Stop prion protein amyloid revealed by solid-state NMR spectroscopy. *Nat. Commun.* **8**, 753
47. Theint, T., Xia, Y., Nadaud, P. S., Mukhopadhyay, D., Schwieters, C. D., Surewicz, K., *et al.* (2018) Structural studies of amyloid fibrils by paramagnetic solid-state nuclear magnetic resonance spectroscopy. *J. Am. Chem. Soc.* **140**, 13161–13166
48. Tycko, R., Savtchenko, R., Ostapchenko, V. G., Makarava, N., and Baskakov, I. V. (2010) The alpha-helical C-terminal domain of full-length recombinant PrP converts to an in-register parallel beta-sheet structure in PrP fibrils: evidence from solid state nuclear magnetic resonance. *Biochemistry* **49**, 9488–9497
49. Shannon, M. D., Theint, T., Mukhopadhyay, D., Surewicz, K., Surewicz, W. K., Marion, D., *et al.* (2019) Conformational dynamics in the core of human Y145Stop prion protein amyloid probed by relaxation dispersion NMR. *Chemphyschem* **20**, 311–317
50. Spagnolli, G., Rigoli, M., Orioli, S., Sevillano, A. M., Faccioli, P., Wille, H., *et al.* (2019) Full atomistic model of prion structure and conversion. *PLoS Pathog.* **15**, e1007864
51. Vazquez-Fernandez, E., Vos, M. R., Afanasyev, P., Cebey, L., Sevillano, A. M., Vidal, E., *et al.* (2016) The structural architecture of an infectious mammalian prion using electron cryomicroscopy. *PLoS Pathog.* **12**, e1005835
52. Saibil, H. R. (2022) Cryo-EM in molecular and cellular biology. *Mol. Cell* **82**, 274–284
53. Bai, X.-C., McMullan, G., and Scheres, S. H. (2015) How cryo-EM is revolutionizing structural biology. *Trends Biochem. Sci.* **40**, 49–57
54. Zielinski, M., Röder, C., and Schröder, G. F. (2021) Challenges in sample preparation and structure determination of amyloids by cryo-EM. *J. Biol. Chem.* **297**, 100938
55. Zhu, Y., Ouyang, Q., and Mao, Y. (2017) A deep convolutional neural network approach to single-particle recognition in cryo-electron microscopy. *BMC Bioinformatics* **18**, 1–10
56. Kimanius, D., Dong, L., Sharov, G., Nakane, T., and Scheres, S. H. (2021) New tools for automated cryo-EM single-particle analysis in RELION-4.0. *Biochem. J.* **478**, 4169–4185
57. Thurber, K. R., Yin, Y., and Tycko, R. (2021) Automated picking of amyloid fibrils from cryo-EM images for helical reconstruction with RELION. *J. Struct. Biol.* **213**, 107736
58. Zivanov, J., Nakane, T., Forsberg, B. O., Kimanius, D., Hagen, W. J., Lindahl, E., *et al.* (2018) New tools for automated high-resolution cryo-EM structure determination in RELION-3. *Elife* **7**, e42166
59. He, S., and Scheres, S. H. (2017) Helical reconstruction in RELION. *J. Struct. Biol.* **198**, 163–176
60. Kimanius, D., Forsberg, B. O., Scheres, S. H., and Lindahl, E. (2016) Accelerated cryo-EM structure determination with parallelisation using GPUs in RELION-2. *Elife* **5**, e18722
61. Glynn, C., Sawaya, M. R., Ge, P., Gallagher-Jones, M., Short, C. W., Bowman, R., *et al.* (2020) Cryo-EM structure of a human prion fibril with a hydrophobic, protease-resistant core. *Nat. Struct. Mol. Biol.* **27**, 417–423
62. Wang, L. Q., Zhao, K., Yuan, H. Y., Wang, Q., Guan, Z., Tao, J., *et al.* (2020) Cryo-EM structure of an amyloid fibril formed by full-length human prion protein. *Nat. Struct. Mol. Biol.* **27**, 598–602
63. Wang, L. Q., Zhao, K., Yuan, H. Y., Li, X. N., Dang, H. B., Ma, Y., *et al.* (2021) Genetic prion disease-related mutation E196K displays a novel amyloid fibril structure revealed by cryo-EM. *Sci. Adv.* **7**, eabg9676
64. preprint Li, Q., Jaroniec, C. P., and Surewicz, W. K. (2021) Cryo-EM structure of disease-related prion fibrils provides insights into seeding barriers. *bioRxiv*. https://doi.org/10.1101/2021.08.10.455830
65. Gallagher-Jones, M., Glynn, C., Boyer, D. R., Martynowycz, M. W., Hernandez, E., Miao, J., *et al.* (2018) Sub-angstrom cryo-EM structure of a prion protofibril reveals a polar clasp. *Nat. Struct. Mol. Biol.* **25**, 131–134
66. Groveman, B. R., Raymond, G. J., Campbell, K. J., Race, B., Raymond, L. D., Hughson, A. G., *et al.* (2017) Role of the central lysine cluster and scrapie templating in the transmissibility of synthetic prion protein aggregates. *PLoS Pathog.* **13**, e1006623
67. Kraus, A., Raymond, G. J., Race, B., Campbell, K. J., Hughson, A. G., Anson, K. J., *et al.* (2017) PrP P102L and nearby lysine mutations

promote spontaneous *in vitro* formation of transmissible prions. *J. Virol.* **91**, e01276
68. Li, Q., Wang, F., Xiao, X., Kim, C., Bohon, J., Kiselar, J., *et al.* (2018) Structural attributes of mammalian prion infectivity: insights from studies with synthetic prions. *J. Biol. Chem.* **293**, 18494–18503
69. Choi, J.-K., Cali, I., Surewicz, K., Kong, Q., Gambetti, P., and Surewicz, W. K. (2016) Amyloid fibrils from the N-terminal prion protein fragment are infectious. *Proc. Natl. Acad. Sci. U. S. A.* **113**, 13851–13856
70. Ghetti, B., Piccardo, P., Frangione, B., Bugiani, O., Giaccone, G., Young, K., *et al.* (1996) Prion protein amyloidosis. *Brain Pathol.* **6**, 127–145
71. Turk, E., Teplow, D. B., Hood, L. E., and Prusiner, S. B. (1988) Purification and properties of the cellular and scrapie hamster prion proteins. *Eur. J. Biochem.* **176**, 21–30
72. Herrmann, L. M., and Caughey, B. (1998) The importance of the disulfide bond in prion protein conversion. *Neuroreport* **9**, 2457–2461
73. Welker, E., Raymond, L. D., Scheraga, H. A., and Caughey, B. (2002) Intramolecular Versus intermolecular disulfide bonds in prion proteins. *J. Biol. Chem.* **277**, 33477–33481
74. preprint Martín-Pastor, M., Codeseira, Y. B., Spagnolli, G., Eraña, H., Fernández, L. C., Martin, D., *et al.* (2021) Solid state NMR reveals a parallel in register architecture for an infectious recombinant prion. *bioRxiv*. https://doi.org/10.1101/2021.07.20.453078
75. Aucoin, D., Xia, Y., Theint, T., Nadaud, P. S., Surewicz, K., Surewicz, W. K., *et al.* (2019) Protein-solvent interfaces in human Y145Stop prion protein amyloid fibrils probed by paramagnetic solid-state NMR spectroscopy. *J. Struct. Biol.* **206**, 36–42
76. Yang, Y., Arseni, D., Zhang, W., Huang, M., Lövestam, S., Schweighauser, M., *et al.* (2022) Cryo-EM structures of amyloid-β 42 filaments from human brains. *Science* **375**, 167–172
77. Shi, Y., Zhang, W., Yang, Y., Murzin, A. G., Falcon, B., Kotecha, A., *et al.* (2021) Structure-based classification of tauopathies. *Nature* **598**, 359–363
78. Sawaya, M. R., Hughes, M. P., Rodriguez, J. A., Riek, R., and Eisenberg, D. S. (2021) The expanding amyloid family: structure, stability, function, and pathogenesis. *Cell* **184**, 4857–4873
79. Chuang, E., Hori, A. M., Hesketh, C. D., and Shorter, J. (2018) Amyloid assembly and disassembly. *J. Cell Sci.* **131**, jcs189928
80. Chatani, E., Yuzu, K., Ohhashi, Y., and Goto, Y. (2021) Current understanding of the structure, stability and dynamic properties of amyloid fibrils. *Int. J. Mol. Sci.* **22**, 4349
81. James, T. L., Liu, H., Ulyanov, N. B., Farr-Jones, S., Zhang, H., Donne, D. G., *et al.* (1997) Solution structure of a 142-residue recombinant prion protein corresponding to the infectious fragment of the scrapie isoform. *Proc. Natl. Acad. Sci. U. S. A.* **94**, 10086–10091
82. Adrover, M., Pauwels, K., Prigent, S., de Chiara, C., Xu, Z., Chapuis, C., *et al.* (2010) Prion Fibrillization is mediated by a native structural element that comprises helices H2 and H3. *J. Biol. Chem.* **285**, 21004–21012
83. Caughey, B., and Raymond, G. J. (1991) The scrapie-associated form of PrP is made from a cell surface precursor that is both protease-and phospholipase-sensitive. *J. Biol. Chem.* **266**, 18217–18223
84. Caughey, B., Raymond, G. J., Ernst, D., and Race, R. E. (1991) N-Terminal truncation of the scrapie-associated form of PrP by lysosomal protease (s): Implications regarding the site of conversion of PrP to the protease-resistant state. *J. Virol.* **65**, 6597–6603
85. Borchelt, D., Taraboulos, A., and Prusiner, S. (1992) Evidence for synthesis of scrapie prion proteins in the endocytic pathway. *J. Biol. Chem.* **267**, 16188–16199
86. Yim, Y.-I., Park, B.-C., Yadavalli, R., Zhao, X., Eisenberg, E., and Greene, L. E. (2015) The multivesicular body is the major internal site of prion conversion. *J. Cell Sci.* **128**, 1434–1443
87. Austin, C. D., Wen, X., Gazzard, L., Nelson, C., Scheller, R. H., and Scales, S. J. (2005) Oxidizing potential of endosomes and lysosomes limits intracellular cleavage of disulfide-based antibody–drug conjugates. *Proc. Natl. Acad. Sci. U. S. A.* **102**, 17987–17992
88. Deleault, N. R., Lucassen, R. W., and Supattapone, S. (2003) RNA molecules stimulate prion protein conversion. *Nature* **425**, 717–720
89. Deleault, N. R., Geoghegan, J. C., Nishina, K., Kascsak, R., Williamson, R. A., and Supattapone, S. (2005) Protease-resistant prion protein amplification reconstituted with partially purified substrates and synthetic polyanions. *J. Biol. Chem.* **280**, 26873–26879
90. Deleault, N. R., Harris, B. T., Rees, J. R., and Supattapone, S. (2007) Formation of native prions from minimal components *in vitro*. *Proc. Natl. Acad. Sci. U. S. A.* **104**, 9741–9746
91. Deleault, N. R., Kascsak, R., Geoghegan, J. C., and Supattapone, S. (2010) Species-dependent differences in cofactor utilization for formation of the protease-resistant prion protein *in vitro*. *Biochemistry* **49**, 3928–3934
92. Deleault, N. R., Piro, J. R., Walsh, D. J., Wang, F., Ma, J., Geoghegan, J. C., *et al.* (2012) Isolation of phosphatidylethanolamine as a solitary cofactor for prion formation in the absence of nucleic acids. *Proc. Natl. Acad. Sci. U. S. A.* **109**, 8546–8551
93. Deleault, N. R., Walsh, D. J., Piro, J. R., Wang, F., Wang, X., Ma, J., *et al.* (2012) Cofactor molecules maintain infectious conformation and restrict strain properties in purified prions. *Proc. Natl. Acad. Sci. U. S. A.* **109**, E1938–E1946
94. Miller, M. B., Wang, D. W., Wang, F., Noble, G. P., Ma, J., Woods, V. L., Jr., *et al.* (2013) Cofactor molecules induce structural transformation during infectious prion formation. *Structure* **21**, 2061–2068
95. Wang, F., Wang, X., Yuan, C. G., and Ma, J. (2010) Generating a prion with bacterially expressed recombinant prion protein. *Science* **327**, 1132–1135
96. Baron, G. S., Wehrly, K., Dorward, D. W., Chesebro, B., and Caughey, B. (2002) Conversion of raft associated prion protein to the protease-resistant state requires insertion of PrP-res (PrP(Sc)) into contiguous membranes. *EMBO J.* **21**, 1031–1040
97. Baron, G. S., and Caughey, B. (2003) Effect of glycosylphosphatidylinositol anchor-dependent and - independent prion protein association with model raft membranes on conversion to the protease-resistant Isoform. *J. Biol. Chem.* **278**, 14883–14892
98. Rouvinski, A., Karniely, S., Kounin, M., Moussa, S., Goldberg, M. D., Warburg, G., *et al.* (2014) Live imaging of prions reveals nascent PrPSc in cell-surface, raft-associated amyloid strings and webs. *J. Cell Biol.* **204**, 423–441
99. Wegmann, S., Miesbauer, M., Winklhofer, K. F., Tatzelt, J., and Muller, D. J. (2008) Observing fibrillar assemblies on scrapie-infected cells. *Pflugers Arch.* **456**, 83–93
100. Rossi, M., Baiardi, S., and Parchi, P. (2019) Understanding prion strains: evidence from studies of the disease forms affecting humans. *Viruses* **11**, 309
101. Klingeborn, M., Race, B., Meade-White, K. D., Rosenke, R., Striebel, J. F., and Chesebro, B. (2011) Crucial role for prion protein membrane anchoring in the neuroinvasion and neural spread of prion infection. *J. Virol.* **85**, 1484–1494
102. Rangel, A., Race, B., Klingeborn, M., Striebel, J., and Chesebro, B. (2013) Unusual cerebral vascular prion protein amyloid distribution in scrapie-infected transgenic mice expressing anchorless prion protein. *Acta Neuropathol. Commun.* **1**, 25
103. Raymond, G. J., Race, B., Hollister, J. R., Offerdahl, D. K., Moore, R. A., Kodali, R., *et al.* (2012) Isolation of novel synthetic prion strains by amplification in transgenic mice coexpressing wild-type and anchorless prion proteins. *J.Virol.* **86**, 11763–11778
104. Race, B., Williams, K., Hughson, A. G., Jansen, C., Parchi, P., Rozemuller, A. J. M., *et al.* (2018) Familial human prion diseases associated with prion protein mutations Y226X and G131V are transmissible to transgenic mice expressing human prion protein. *Acta Neuropathol. Commun.* **6**, 13
105. Baron, G. S., Hughson, A. G., Raymond, G. J., Offerdahl, D. K., Barton, K. A., Raymond, L. D., *et al.* (2011) Effect of glycans and the glycophosphatidylinositol anchor on strain dependent conformations of scrapie prion protein: Improved purifications and infrared spectra. *Biochemistry* **50**, 4479–4490
106. Mahal, S. P., Jablonski, J., Suponitsky-Kroyter, I., Oelschlegel, A. M., Herva, M. E., Oldstone, M., *et al.* (2012) Propagation of RML prions in mice expressing PrP devoid of GPI anchor leads to formation of a novel, stable prion strain. *PLoS.Pathog.* **8**, e1002746

107. Aguilar-Calvo, P., Xiao, X., Bett, C., Eraña, H., Soldau, K., Castilla, J., *et al.* (2017) Post-translational modifications in PrP expand the conformational diversity of prions *in vivo*. *Sci. Rep.* **7**, 1–15
108. Sevillano, A. M., Aguilar-Calvo, P., Kurt, T. D., Lawrence, J. A., Soldau, K., Nam, T. H., *et al.* (2020) Prion protein glycans reduce intracerebral fibril formation and spongiosis in prion disease. *J. Clin. Invest.* **130**, 1350–1362
109. Bett, C., Kurt, T. D., Lucero, M., Trejo, M., Rozemuller, A. J., Kong, Q., *et al.* (2013) Defining the conformational features of anchorless, poorly neuroinvasive prions. *PLoS Pathog.* **9**, e1003280
110. Cancellotti, E., Bradford, B. M., Tuzi, N. L., Hickey, R. D., Brown, D., Brown, K. L., *et al.* (2010) Glycosylation of PrPC determines timing of neuroinvasion and targeting in the brain following transmissible spongiform encephalopathy infection by a peripheral route. *J. Virol.* **84**, 3464–3475
111. Wiseman, F. K., Cancellotti, E., Piccardo, P., Iremonger, K., Boyle, A., Brown, D., *et al.* (2015) The glycosylation status of PrPC is a key factor in determining transmissible spongiform encephalopathy transmission between species. *J. Virol.* **89**, 4738–4747
112. Makarava, N., Chang, J. C., Molesworth, K., and Baskakov, I. V. (2020) Posttranslational modifications define course of prion strain adaptation and disease phenotype. *J. Clin. Invest.* **130**, 4382–4395
113. Kraus, A., Groveman, B. R., and Caughey, B. (2013) Prions and the potential transmissibility of protein misfolding diseases. *Annu. Rev. Microbiol.* **67**, 543–564
114. Gousset, K., Schiff, E., Langevin, C., Marijanovic, Z., Caputo, A., Browman, D. T., *et al.* (2009) Prions hijack tunnelling nanotubes for intercellular spread. *Nat. Cell Biol.* **11**, 328–336
115. Vassileff, N., Cheng, L., and Hill, A. F. (2020) Extracellular vesicles - propagators of neuropathology and sources of potential biomarkers and therapeutics for neurodegenerative diseases. *J. Cell Sci.* **133**, jcs243139
116. Rangel, A., Race, B., Phillips, K., Striebel, J., Kurtz, N., and Chesebro, B. (2014) Distinct patterns of spread of prion infection in brains of mice expressing anchorless or anchored forms of prion protein. *Acta Neuropathol. Commun.* **2**, 1–14
117. Houston, F., and Andreoletti, O. (2019) Animal prion diseases: the risks to human health. *Brain Pathol.* **29**, 248–262
118. Race, B., Williams, K., Orru, C. D., Hughson, A. G., Lubke, L., and Chesebro, B. (2018) Lack of transmission of chronic wasting disease to cynomolgus macaques. *J. Virol.* **92**, e00550-18
119. Wang, Z., Qin, K., Camacho, M. V., Cali, I., Yuan, J., Shen, P., *et al.* (2021) Generation of human chronic wasting disease in transgenic mice. *Acta Neuropathol. Commun.* **9**, 158
120. Bossers, A., Belt, P. B. G. M., Raymond, G. J., Caughey, B., de Vries, R., and Smits, M. A. (1997) Scrapie susceptibility-linked polymorphisms modulate the *in vitro* conversion of sheep prion protein to protease-resistant forms. *Proc. Natl. Acad. Sci. U. S. A.* **94**, 4931–4936
121. Kocisko, D. A., Priola, S. A., Raymond, G. J., Chesebro, B., Lansbury, P. T., Jr., and Caughey, B. (1995) Species specificity in the cell-free conversion of prion protein to protease-resistant forms: A model for the scrapie species barrier. *Proc. Natl. Acad. Sci. U. S. A.* **92**, 3923–3927
122. Priola, S. A., Caughey, B., Race, R. E., and Chesebro, B. (1994) Heterologous PrP molecules interfere with accumulation of protease-resistant PrP in scrapie-infected murine neuroblastoma cells. *J.Virol.* **68**, 4873–4878
123. Prusiner, S. B., Scott, M., Foster, D., Pan, K. M., Groth, D., Mirenda, C., *et al.* (1990) Transgenetic studies implicate interactions between homologous PrP isoforms in scrapie prion replication. *Cell* **63**, 673–686
124. Raymond, G. J., Bossers, A., Raymond, L. D., O'Rourke, K. I., McHolland, L. E., Bryant, P. K., III, *et al.* (2000) Evidence of a molecular barrier limiting susceptibility of humans, cattle and sheep to chronic wasting disease. *EMBO J.* **19**, 4425–4430
125. Raymond, G. J., Hope, J., Kocisko, D. A., Priola, S. A., Raymond, L. D., Bossers, A., *et al.* (1997) Molecular assessment of the transmissibilities of BSE and scrapie to humans. *Nature* **388**, 285–288
126. Scott, M., Groth, D., Foster, D., Torchia, M., Yang, S. L., DeArmond, S. J., *et al.* (1993) Propagation of prions with artificial properties in transgenic mice expressing chimeric PrP genes. *Cell* **73**, 979–988
127. Goldmann, W., Hunter, N., Smith, G., Foster, J., and Hope, J. (1994) PrP genotype and agent effects in scrapie: change in allelic interaction with different isolates of agent in sheep, a natural host of scrapie. *J. Gen. Virol.* **75**, 989–995
128. Mead, S., Whitfield, J., Poulter, M., Shah, P., Uphill, J., Campbell, T., *et al.* (2009) A novel protective prion protein variant that colocalizes with kuru exposure. *New Engl. J. Med.* **361**, 2056–2065
129. Asante, E. A., Smidak, M., Grimshaw, A., Houghton, R., Tomlinson, A., Jeelani, A., *et al.* (2015) A naturally occurring variant of the human prion protein completely prevents prion disease. *Nature* **522**, 478–481
130. Priola, S. A., and Chesebro, B. (1995) A single hamster amino acid blocks conversion to protease-resistant PrP in scrapie-infected mouse neuroblastoma cells. *J. Virol.* **69**, 7754–7758
131. Priola, S. A., Chabry, J.l., and Chan, K. (2001) Efficient conversion of normal prion protein (PrP) by abnormal hamster PrP is determined by homology at amino acid residue 155. *J. Virol.* **75**, 4673–4680